JAMES | Journal of Advances in Modeling Earth Systems

RESEARCH ARTICLE
10.1029/2018MS001451

# The Vertical Momentum Budget of Shallow Cumulus Convection: Insights From a Lagrangian Perspective

**Yang Tian[1], Zhiming Kuang[1,2], Martin S. Singh[3], and Ji Nie[4]**

[1]Department of Earth and Planetary Sciences, Harvard University, Cambridge, MA, USA, [2]John A. Paulson School of Engineering and Applied Sciences, Harvard University, Cambridge, MA, USA, [3]School of Earth, Atmosphere and Environment, Monash University, Clayton, VIC, Australia, [4]School of Physics, Peking University, Beijing, China

**Abstract** A Lagrangian Particle Dispersion Model is embedded into large eddy simulations to diagnose the responses of shallow cumulus convection to a small-amplitude large-scale temperature perturbation. The Lagrangian framework allows for a decomposition of the vertical momentum budget and diagnosis of the forces that regulate cloudy updrafts. The results are used to shed light on the parameterization of vertical velocity in convective schemes, where the treatment of the effects of entrainment as well as buoyancy-induced and mechanically induced pressure gradients remains highly uncertain. We show that both buoyancy-induced and mechanically induced pressure gradients are important for the vertical momentum budget of cloudy updrafts, whereas the entrainment dilution term is relatively less important. Based on the analysis of the dominant force balance, we propose a simple model to derive the perturbation pressure gradient forces. We further illustrate that the effective buoyancy and dynamic perturbation pressure can be approximated to a good extent using a simple cylindrical updraft model given the cloud radius. This finding has the potential for improving the parameterization of vertical velocity in convective schemes and the development of a unified scheme for cumulus convection.

**Plain Language Summary** This article employed a new approach to understand what regulates in-cloud vertical velocity distribution, the understanding of which has important implications for improving severe weather predictions such as hail and lightning. Furthermore, a simple cartoon model was proposed to calculate perturbation pressure terms in vertical velocity budget, which allows for advancement in representing clouds in climate models.

**Key Points:**
- Perturbation pressure terms are important in vertical momentum budget, which are the dominant sink of vertical momentum
- Both buoyancy-induced and mechanically induced pressure gradients are equally important, therefore should be included in vertical velocity equation
- We illustrate that a simple updraft model can be employed to explicitly calculate perturbation pressure terms given a reasonable cloud size

**Supporting Information:**
- Supporting Information S1

**Correspondence to:**
Y. Tian,
yangtian@fas.harvard.edu

**Citation:**
Tian, Y., Kuang, Z., Singh, M., & Nie, J. (2019). The vertical momentum budget of shallow cumulus convection: Insights from a Lagrangian perspective. *Journal of Advances in Modeling Earth Systems*, *11*, 113–126. https://doi.org/10.1029/2018MS001451

Received 19 JUL 2018
Accepted 22 DEC 2018
Accepted article online 28 DEC 2018
Published online 15 JAN 2019



## 1. Introduction

In-cloud vertical velocity is an important cloud property. It is a direct measure of convective strength and has a strong influence on cloud microphysics. High vertical velocity contributes to high supersaturation inside clouds, which allows for a larger fraction of cloud condensation nuclei to be activated. Clouds with high vertical velocities can loft more ice particles and are therefore often associated with high-impact weather events such as hail (Danielsen et al., 1972) and lightning (e.g., Price & Rind, 1992; Williams et al., 1989). In-cloud velocity also influences convective overshooting and tropospheric-stratospheric exchange (e.g., Hsu & Prather, 2014).

Compared to traditional convective parameterizations based purely on mass flux (e.g., Arakawa & Schubert, 1974; Tiedtke, 1989), parameterizations that explicitly include cloud-scale velocity are advantageous for a number of reasons (e.g., Bretherton et al., 2004; De Rooy & Siebesma, 2010; Neggers et al., 2009). For example, vertical velocity can serve as a trigger for the occurrence of moist convection that naturally connects dry thermals in the subcloud layer with moist updrafts in the cloud layer; the cloud-top height can be determined more realistically as the height at which the in-cloud vertical velocity vanishes (Neggers et al., 2009; Siebesma et al., 2007; Soares et al., 2004); and the application of a vertical velocity equation in cloudy updrafts allows for tighter coupling between microphysical and dynamical processes (de Roode et al., 2012).

Updraft vertical velocity is commonly parameterized using an equation of the form

$$\frac{1}{2}\frac{\partial w_c^2}{\partial z} = aB_c - b\epsilon w_c^2, \tag{1}$$

where subscript $c$ indicates in-cloud properties, $B$ is the buoyancy, and $\epsilon$ is the lateral entrainment rate. The left-hand side of equation (1) represents vertical advection (total acceleration for steady-state plumes), whereas the effects of the pressure gradient force and subplume turbulent fluxes are incorporated by the choice of the proportionality constants $a$ and $b$ into the buoyancy and the entrainment terms, respectively (e.g., Gregory, 2001; Neggers et al., 2009; Simpson & Wiggert, 1969). A discussion of how equation (1) can be rationalized can be found in de Roode et al. (2012).

Previous studies have generally determined the proportionality factors $a$ and $b$ using an empirical fitting procedure, and the values chosen differ depending on the observational data used to construct the empirical fit and the specific form of the equation used. For example, the $b$ coefficient can vary by more than a factor of 3 with different observational data (e.g., de Roode et al., 2012). Moreover, a comprehensive understanding of the dominant balance of forces that regulates the vertical velocity distribution within convective updrafts is still lacking. Sherwood et al. (2013) referred to cloud thermals as "slippery" because they found that the entrainment dilution associated with cloud thermals is relatively small compared to buoyancy, therefore the dominant balance in a mature cloud thermal is between its buoyancy and acceleration. However, through tracking thousands of clouds generated in large eddy simulations (LES), Romps and Charn (2015) argued that buoyancy is mostly balanced by drag force, thus cloud thermals should be "sticky" rather than slippery.

Here we apply a Lagrangian approach to better understand the vertical momentum budget of shallow cumulus convection as represented in LES. The new approach examines cumulus convection from a plume-spectrum perspective. Lagrangian particle tracking reveals all necessary dynamical information along each particle's trajectory, the evolution history of each term, and their relative accumulative contribution from cloud base upward, thus allowing for an unambiguous assessment of their roles in determining the vertical momentum of cloudy updrafts. We also calculate the fractional entrainment rate and its contribution to the vertical momentum budget directly from a Lagrangian view, instead of treating this term as a residual as done in most budget analysis (e.g., de Roode et al., 2012). Based on the relative importance of different terms, we can assess what should be the dominant force balance and infer the most important terms to include to parameterize vertical velocity inside the cloudy updrafts. More importantly, we explore the potential of assuming a simple shape (i.e., a deterministic cartoon) for cloudy updrafts to compute the values of $a$ and $b$ without arbitrarily predefining their values for different convective cases, given the knowledge of cloud radius.

We shall further quantify the responses of various terms in the vertical momentum budget to external temperature perturbations within a linear response framework, similar to what has been done in, for example, Tompkins and Craig (1998), Kuang (2010), Tulich and Mapes (2010), Nie and Kuang (2012a), and Tian and Kuang (2016). By applying specified temperature perturbations and observing the responses in various forcings, we can better understand the processes and factors that determine these forcings, as done for fractional entrainment rate in Tian and Kuang (2016). For simplicity, we will focus on the responses of shallow nonprecipitating cumuli to a small temperature perturbation. Nie and Kuang (2012a) examined the responses of shallow cumulus to temperature and moisture perturbations using the technique of tracer encoding and with the aid of a stochastic parcel model. Here we embed a large number of Lagrangian particles (parcels) in the LES simulations (see supporting information for model details). Combining the trajectories of the parcels with the snapshots of the LES output provides a full history of parcel properties along their trajectories, enabling a Lagrangian perspective on cumulus scale dynamics (e.g., Heus, 2008; Nie & Kuang, 2012b; Torri et al., 2015; Weil, 2004; Yeo & Romps, 2013). By casting Lagrangian particles into a spectrum of plumes, we represent cumulus ensembles in a way most relevant to convective parameterization.

Shallow cumulus convection is comparatively simpler than deep convection because it does not involve complications associated with precipitation. Despite a simpler dynamics, shallow convection shares similar cloud ensemble characteristics as deep convection (Kuang & Bretherton, 2006) and captures a number of the important interactions between subcloud layer and free troposphere, cloud and environment, and within clouds themselves. Shallow, nonprecipitating convection thus serves as a good starting point for understanding in-cloud vertical velocity.

Section 2 briefly describes the model used and the experimental design. The analysis methods, results, and their interpretations are presented in section 3, followed by a summary in section 4.

## 2. Models and Experimental Design

We performed LES using the System for Atmospheric Modeling (SAM) version 6.8.2 (Khairoutdinov & Randall, 2001) for the undisturbed phase of the Barbados Oceanographic and Meteorological Experiment (Holland & Rasmusson, 1973). Readers are referred to Khairoutdinov and Randall (2001) for a description of the equations solved in the SAM. The basic model setup and analysis methods are the same as those in Tian and Kuang (2016) except for two major modifications: we adopt a 25-m horizontal resolution to better resolve small-scale eddies, and we impose time-invariant temperature and moisture tendencies to maintain the basic environmental state as described below. Briefly speaking, SAM was run on a doubly periodic domain ($6.4 \times 6.4$ km) with 128 vertical layers and with a 25-m grid spacing in both horizontal and vertical directions. The simulation was initially spun up for 3 hr until the cloud field reached a statistically steady state. Restart files were then saved from the final state of the control simulation every 5 min (at hour 3, hour 3 + 5 min, hour 3 + 10 min, etc.) to generate an ensemble of 24 control runs. We then introduced a small-amplitude temperature perturbation (horizontally uniform, Gaussian-shaped in height, centered at 975 m with a half-width of 75 m and a peak value of +0.25 K) to create an additional set of 24 perturbed runs, which start from the same fully developed cumulus fields as the control runs but with the added temperature perturbation. The perturbation experiment helps probe the sensitivity of different terms in the vertical momentum budget under a linear response framework, making the statistical inferences more robust (e.g., Tian & Kuang, 2018). The size of the temperature perturbation was chosen by balancing the need for a good signal-to-noise ratio, which favors large perturbations, and the need for the response to remain mostly linear, which favors small perturbations. The perturbation height was chosen to give the best signal-to-noise ratio, and it should be above the subcloud layer to avoid complication of boundary layer dynamics. Adopting an ensemble approach increases the sample size and enables us to calculate robust differences between the control and perturbed simulations. Each control and perturbed pair was run for half an hour with seeded particles, and model statistics were output every 4 s. We analyzed the convective responses of shallow cumuli to the added perturbation by comparing the results of the paired simulations. The perturbation experiment helps probe the sensitivity of different terms within the vertical momentum equation, it also serves as an additional test case for our vertical velocity parameterization. As convection responds to remove the initial temperature anomaly, the amplitude of the initially added warm anomaly gradually decreases over time. Since we want to examine the initial response of the convective ensemble to the large-scale temperature perturbation without the interference of the feedback from the convective heating itself, we added time-independent heating and moistening tendencies to counteract the model drift. These tendencies were obtained by subtracting drifting rates of temperature and humidity over the half hour period from the initial large-scale forcing, and this process was carried out iteratively until the adjustment was small.

## 3. Analysis and Results

### 3.1. Vertical Momentum Response to the Temperature Perturbation

The numerically simulated cumulus ensembles were cast in terms of an ensemble of entraining plumes as in, for example, Lin and Arakawa (1997) and Kuang and Bretherton (2006). This is achieved by tracking a large number of Lagrangian particles (~30 million) embedded in the LES (see supporting information for more particle model details). The particles are released in the height range between the surface and ~2 km, and they are uniformly distributed within this domain. Cloudy particles are grouped by the height at which they eventually detrain from the cloud. Here we define a detrainment event as occurring when particles exit from cloudy updrafts to the environment and stay in the environment for at least a minute. Particles detraining at the same heights are grouped as one "entraining plume" or one "parcel group." Therefore, the term entraining plume used here should not be confused with the similarity plumes described in previous water tank experiments (Morton et al., 1956). Instead, a "plume" is composed of parcels from different clouds and parcels from a single cloud contribute to multiple "plumes". In this study a relatively large number (100) of parcel groups is adopted to enhance the homogeneity within each group while exposing differences between groups. Using our parcel grouping method, parcels belonging to the same group in the control and perturbed runs may be viewed as the same parcel in a statistical sense, and the averaged differences between these pairs of runs over the half an hour simulation period are taken as the convective responses to the imposed temperature perturbation. The above procedure is the same as in Tian and Kuang (2016) and summarized here for completeness. Each of the parcel groups may be considered as an analogue of a plume within a spectral plume representation of convection (Arakawa & Schubert, 1974), which can take

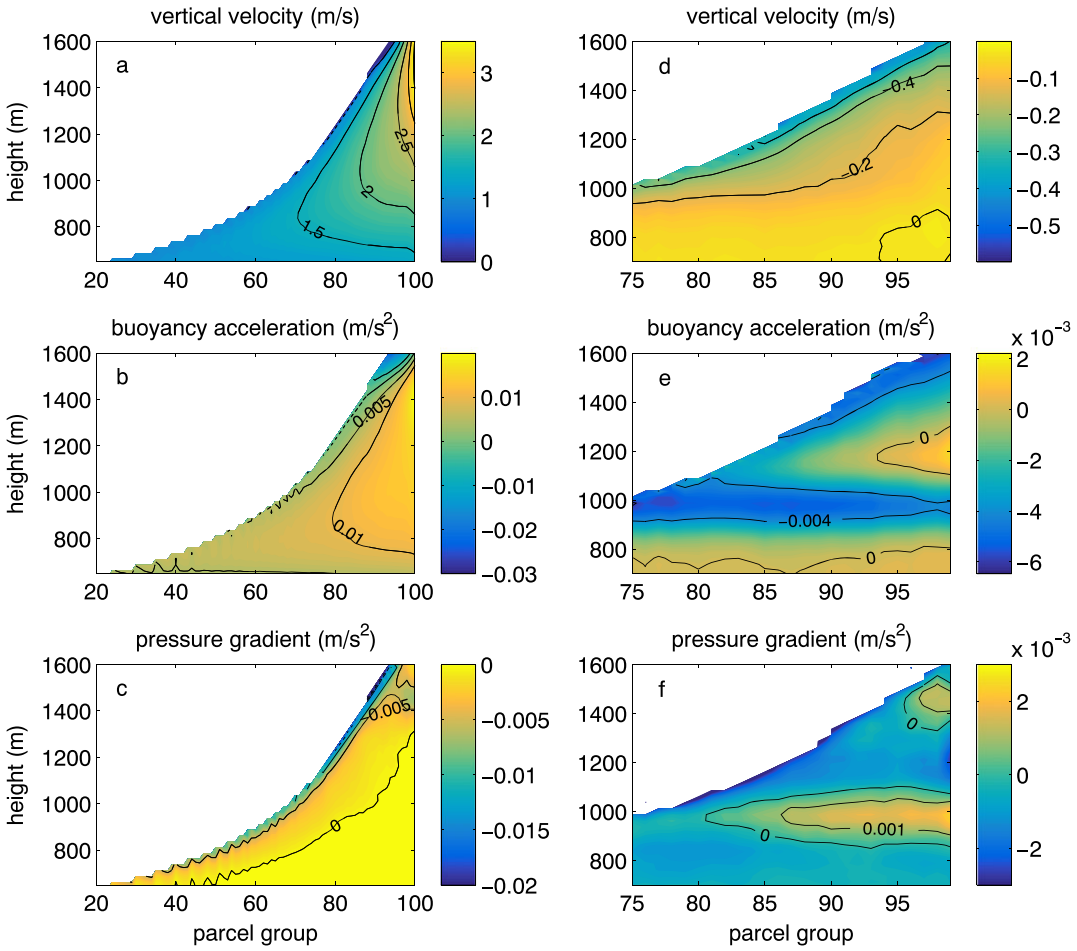


**Figure 1.** (left) Control run cloudy updraft (a) vertical velocity, (b) buoyancy acceleration, (c) acceleration due to pressure gradient force $-\frac{1}{\rho_0}\frac{dp'}{dz}$ , as functions of parcel group and height (see text for details on how the parcel groups are defined); (right) (d)-(f) the same as the left column but for the differences between the ensemble perturbed and control runs for higher-reaching parcel groups.

into account in-cloud heterogeneity. At the same time, summing over all parcel groups can recover the bulk plume properties. Therefore, the spectral plume model can be more versatile than the bulk plume representation (Lin & Arakawa, 1997), the latter being the basis for setting coefficients $a$ and $b$ in equation (1). We are interested in the cloudy updrafts, and cloudy updrafts are defined to be grid boxes with vertical velocity greater than 1 m/s and nonprecipitating liquid water mixing ratio greater than 0.01 g/kg. Cloudy particles are those Lagrangian particles that are within the cloudy updrafts. The results are not sensitive to this criterion.

The general dynamical properties of cloudy updrafts and their convective responses are shown in Figure 1. Since all particles are grouped based on the percentile of their detrainment heights, and those detrainment heights are equally divided into 100 groups in ascending order, each percentile has the same number of particles, and larger parcel group numbers represent higher detrainment levels. For the convective responses, we focus on the parcel groups that are most affected by the added perturbation (parcel group 75 and larger), and we neglect those parcel groups that do not reach above the perturbation layer. Buoyancy acceleration (Figure 1b) is almost uniform across all parcel groups at the cloud base (~650 m), whereas slightly higher vertical velocity (Figure 1a) is observed for those parcel groups that detrain higher, indicating a role for initial conditions at cloud base in determining the fate of cloudy parcels. The profile of vertical velocity peaks at the base of the trade inversion (~1,500 m), which is also the level at which the buoyancy acceleration crosses zero and becomes negative above.

In the perturbed simulations, the imposed warm anomaly acts as a buoyancy barrier (Figure 1e) that strongly reduces the kinetic energy of all parcel groups, but less so for higher-reaching parcel groups (Figures 1d and 1e). The pressure gradient term has similar order of magnitude as the buoyancy acceleration (Figure 1c); it is mostly negative in the cloudy updraft and partially balances the buoyancy term, and it becomes less negative inside the perturbation layer in response to the added temperature perturbation (Figure 1f). Similar results were shown in Tian and Kuang (2016) but at a lower resolution. In the following sections, we will show in more detail the relative importance of different terms in determining the vertical momentum budget from a linear response perspective: first, we introduce a new way of calculating the fractional entrainment rate by using Lagrangian particles. We then determine the dominant force balance in the momentum equation. Lastly, we propose a deterministic cartoon model to parameterize vertical velocity in large-scale models.

### 3.2. Distribution-Based Approach to Defining Entrainment

Some entrainment studies thus far have included, in their calculation of entrainment and detrainment rates, the fast cycling of air parcels between the cloud and the environment categories (Dawe & Austin, 2013; Romps, 2010). However, this tends to lead to artificially high estimates of the entrainment rate because these fast-cycling particles have similar properties to the clouds themselves, and they therefore contribute little to changes in cloud properties (Yeo & Romps, 2013). To ameliorate the effects of rapid cycling between clouds and clear air, some studies enforce a minimum time over which the entrained air must remain inside the cloud or create a buffer zone surrounding the clouds that is included in the definition of the "cloudy region" (e.g., Nie & Kuang, 2012b; Romps & Kuang, 2010; Tian & Kuang, 2016). Here we employ a new approach to diagnose entrainment amount and associated properties. The purpose here is to further reduce the arbitrariness of prescribing a residence time/buffer zone, and also to provide an independent validation of the previously calculated fractional entrainment rate as in Tian and Kuang (2016). The underlying assumption behind this approach is that, in a Lagrangian framework, if we track in-cloud particles backward for a sufficient amount of time, the particles originating from the environment will reach positions and take properties that are relatively stable, aside from changes associated with passing gravity waves and the slow descent in the environment. Using this assumption and the tracked Lagrangian trajectories, we can obtain a more objective identification of entrainment sources that faithfully records the entrained properties that are inputs for any entraining-plume based parameterization of convection.

The Lagrangian-based approach is carried out in the following way: for each parcel group, we select a height that is 50 m (the results are independent of this height choice as long as it is close to the detrainment height) below the detrainment height in the perturbed case (because particles generally detrain at lower levels in the perturbed runs), then track all cloudy particles from that height backward in time until their thermodynamic properties and their vertical positions become relatively stable in time. To examine this more closely, we select the ninetieth percentile among all parcel groups to demonstrate this stable distribution approach since the behavior of this parcel group is representative of the general convective responses (and other higher-reaching parcel groups) that we see in Figure 1. Recall that the ninetieth parcel group is composed of particles reaching a detrainment height that ranks in the ninetieth percentile among all parcel groups. Figure 2 shows the particle distributions as a function of total water $q_t$ and vertical velocity $w$ at various times before they enter our chosen height (results for 1,200 to 1,400 s are not shown because distributions change little visually for those tracking times), and the distribution is binned into entrained properties. The two axes can be any other variables such as height or $\theta_e$. We chose $q_t$ and $w$ because background $q_t$ is a thermodynamic variable that decreases monotonically with height in this nonprecipitating shallow convection case, and $w$ is the dynamic variable that we focus on in this study. The distribution of the tracked particles changes rapidly at first, but for tracking times longer than 600 s, the distribution becomes relatively stable. Tracking back to 1,400 s gives a very stable distribution so that an increase in tracking time has little effect on the entrained properties, and the difference between adjacent time slices is negligible (not shown here). In-cloud particles mainly have two origins: the subcloud layer and the clear environment in the cloud layer. The particle distribution is relatively compact in the subcloud layer with total water mixing ratio around 17 g/kg and vertical velocity about 0.5 m/s, slightly smaller than the lower limit for cloudy updrafts defined in this work. Other particles that are entrained from the environment laterally take corresponding environmental total water content values and near-zero vertical velocities, which is also typical for environmental air. The fractional entrainment rate calculated from this approach is similar to the previous approach that requires entrained particles to stay in the clouds for over 1 min as in Tian and Kuang (2016), but this method

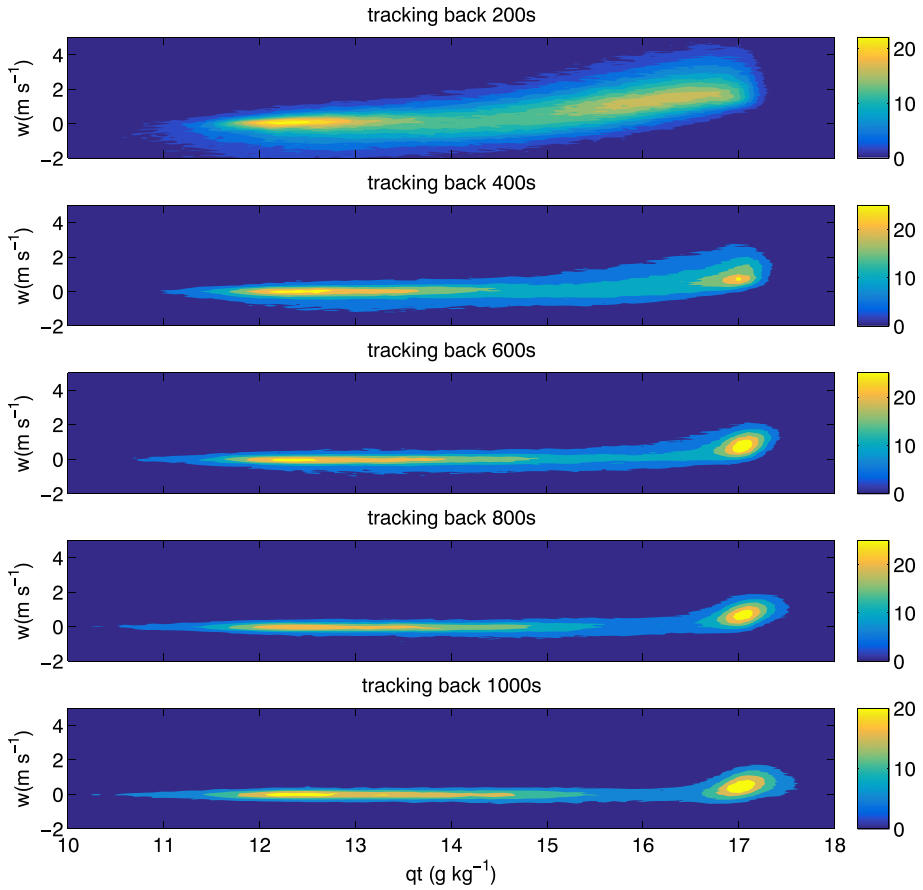


**Figure 2.** Particle number distribution when tracking back for 200, 400, 600, 800, 1,000 s as a function of vertical velocity w and total water content qt for the ninetieth percentile parcel group. The values take the initial vertical velocity and total water content, and shown here as the square root of the original values for illustration purpose.

provides a more objective way to get the original properties of the entrained air than defining entrainment as an instantaneous event.

Next we use this entrainment definition to reconstruct the momentum budget from a Lagrangian perspective.

### 3.3. Reconstruction of Momentum Budget

We demonstrate the Lagrangian reconstruction of momentum budget with parcel group 90. We have neglected the turbulent diffusion term because it is almost negligible in the momentum budget. Entrainment amount and entrained properties are based on the distributions of Lagrangian particles when they are tracked back 1,400 s. Because the total simulation time is 30 min, the longer we track back, the fewer particles will be sampled. We have chosen 1,400 s because the distributions in the entrained property change little beyond this time lag, and at the same time there are still sufficient particles to ensure statistical significance. Lagrangian vertical velocity for a given layer is obtained by averaging the vertical velocity of all particles at that layer (see supporting information for a comparison between Lagrangian and Eulerian vertical velocity), and the vertical velocity for each individual particle is calculated as follows: sample all the particles at the selected layer and then trace them back 1,400 s to their original locations; record their initial vertical velocities and move forward along the trajectories and update the vertical velocities with acceleration terms (equation (2)). For the $i$th particle:

$$w_i(t) = w_i(t_0) + \int_{t_0}^{t} F_i(t')dt', \tag{2}$$

$$F_i(t') = B_i(t') - \frac{dp_i'(t')}{\rho_0 dz}. \tag{3}$$

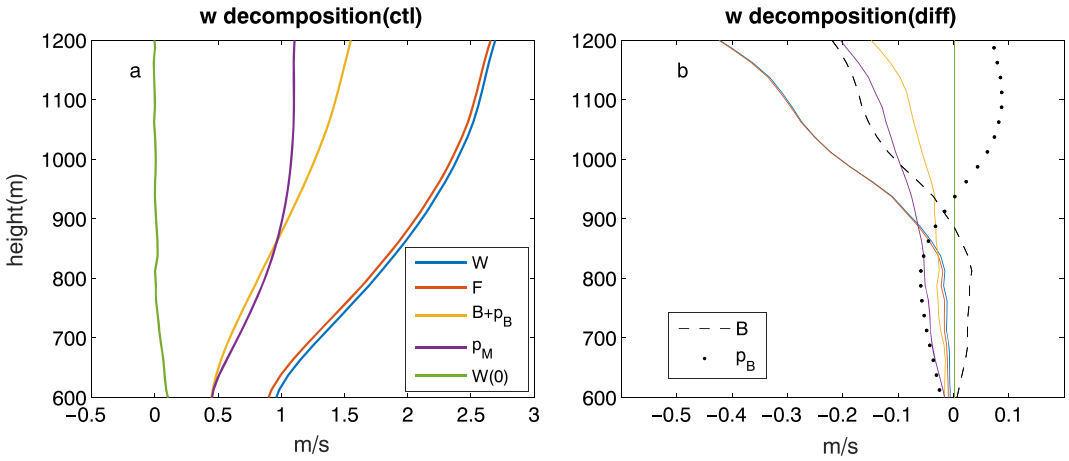


**Figure 3.** (a) Vertical velocity decomposition for the ninetieth percentile parcel group control run: blue curve(w) = total vertical velocity predicted from Lagrangian tracking; red(F) = integrated contribution from total acceleration, including both buoyancy acceleration and pressure gradient term; orange(B+$p_B$) = contribution from total buoyancy forcing term, which is composed of both buoyancy and pressure gradient term, here $p_B$ represents $-\frac{1}{\rho_0}\frac{dp'_B}{dz}$ term integrated over time; purple($p_M$) = contribution from total mechanical forcing $-\frac{1}{\rho_0}\frac{dp'_M}{dz}$; green($w(t_0)$) = entrained initial vertical velocity based on the stable distribution when tracked back 1,400 s; (b) same as (a) but for differences between perturbed and control run, representing convective responses due to the added warm anomaly. The B (black dashed line) and $p_B$ (black dotted line) are plotted separately to show the effect of cancelation between the two.

Here $w(t)$ is the particle vertical velocity at time $t$; $t_0$ is the time 1,400 s before the particle enters our selected layer; $p'$ is the perturbation pressure, which is relative to the anelastic basic state; $F$ is the total acceleration term, subscript $i$ refers to the $i$th particle; and $\rho_0$ is the reference density at a given height. Initial vertical velocity is linearly interpolated to the particle position (1-D interpolation in each direction). The acceleration term is taken from the LES snapshot, which is composed of both buoyancy acceleration and acceleration from the pressure gradient force. The acceleration value assigned to each particle takes the grid-mean value of the grid box it resides in.

Figure 3 demonstrates the vertical velocity decomposition into various terms for parcel group 90. The left panel is for control run ensemble averages and the right panel shows the change in the perturbed run relative to the control run (perturbed minus control). For illustration purpose, different terms in the vertical momentum equation have all been converted to velocity unit (m/s), that is, the acceleration terms are integrated until the particle reaches the selected height. Therefore, the value for each component essentially represents the mass-weighted vertical velocity that particles would assume without contributions from the other components. Entrained vertical velocity is accounted for by the averaged initial vertical velocity of parcels per vertical level ($w(t_0)$ in equation (2)), and the initial velocity generally falls close to zero, which is a clear indication that our methodology is picking the correct level for the origin of entrained particles. However, we should point out that the green line in Figure 3a does not represent the total entrainment effect since the entrainment term also modifies the thermodynamic properties of the updraft, thus its buoyancy and associated acceleration terms. With near-zero entrained initial vertical velocity, the contribution from mass-weighted acceleration terms is expected to be close to that of total velocity (Figure 3a). We can further partition the pressure gradient term into buoyancy-induced ($p'_B$) and mechanically induced ($p'_M$) components. The pressure gradients $p'_B$ and $p'_M$ are defined as the solutions of Poisson equations (see, e.g., the textbook by Houze, 1994):

$$\nabla^2 p'_B = \partial_z(\rho_0 B), \tag{4}$$

$$\nabla^2 p'_M = -\nabla\cdot(\rho_0\vec{v}\cdot\nabla\vec{v}). \tag{5}$$

In the above expressions, $\nabla$ is a 3-D Laplace operator, and $\vec{v}$ is the 3-D velocity vector. We define the thermodynamic (total buoyancy) forcing to be the sum of buoyancy acceleration B and its induced pressure gradient term$-\frac{1}{\rho_0}\frac{dp'_B}{dz}$, the dynamical (total mechanical) forcing $-\frac{1}{\rho_0}\frac{dp'_M}{dz}$ is used to represent the dynamic per-

turbation pressure due to the divergence of the advective momentum flux. As illustrated in Figure 3a, both thermodynamic and dynamical forcing contribute to the total acceleration of cloudy updrafts in the control run, with the magnitude of thermodynamic forcing being slightly larger than that of the mechanical forcing. The initial vertical velocity $w(t_0)$ varies little between perturbed and control runs, so the difference is close to zero (Figure 3b). The difference in buoyancy acceleration (B) is strongly balanced by the difference in the buoyancy-induced pressure gradient term, leading to reduced net effect on the updraft vertical velocity (Figure 3b). This is known as the virtual mass effect, and the extent of the buoyancy reduction by this mechanism depends on the aspect ratio of the updraft (e.g., Davies-Jones, 2003; Morrison, 2016a). Because the buoyancy-driven pressure gradient term is strongly tied to the cloud size parameters, the larger the surface area, the more inertia a cloudy updraft experiences by pushing air to its surrounding. The vertical momentum advection is also greatly reduced due to the buoyancy barrier. Our decomposition method thus clearly demonstrates the relative importance between total buoyancy forcing and mechanical forcing, given that both terms are diluted equally by the same amount of entrainment, they can be compared against each other directly. The results are consistent with Romps and Charn (2015) who found that both buoyancy and pressure gradient forces play important roles in determining the updraft vertical velocity, and they should both be considered in parameterizing vertical velocity in convective parameterizations.

### 3.4. Simple Model for Perturbation Pressure in Vertical Momentum Budget

Since both buoyancy and pressure gradient forces play important roles in determining the updraft velocity, in this section we demonstrate how we could potentially use a simple cloudy updraft model to calculate perturbation pressure in the vertical momentum budget. By summing equation (2) over all parcels within a group, we can form an equation for the total vertical momentum (per unit mass) within the parcel group,

$$\sum_{i=1}^{N(z)} w_i(z) = \sum_{i=1}^{N(z-\Delta z)} \left(w_i(z-\Delta z) + \int_{t(z-\Delta z)}^{t(z)} F_i(t)dt\right) + \sum_{i=1}^{N_e(z)} w_{ei}(z), \tag{6}$$

where $\Delta z$ is a finite vertical distance; $w_i(z)$ and $w_i(z-\Delta z)$ refer to the vertical velocities of particle $i$ at heights $z$ and $z-\Delta z$, respectively; $N(z)$ is the total particle number at height $z$ within the group; $N(z-\Delta z)$ is the total particle number at height $z-\Delta z$; and $N_e(z) = N(z) - N(z-\Delta z)$ is the number of particles entrained into the parcel group between heights $z-\Delta z$ and $z$. The vertical velocity of those entrained particles is denoted as $w_e(z)$. The second term on the right-hand side (r.h.s.) $\sum_{i=1}^{N(z-\Delta z)} \int_{t(z-\Delta z)}^{t(z)} F(t)dt$ is the sum of acceleration over all particles when they ascend from height $z-\Delta z$ to $z$. Now we introduce the average operator, in which the overbar indicates averaged properties of related particles within a subplume (parcel group): $\bar{w}(z) = \frac{\sum_{i=1}^{N(z)} w_i(z)}{N(z)}$, $\bar{w}(z-\Delta z) = \frac{\sum_{i=1}^{N(z-\Delta z)} w_i(z-\Delta z)}{N(z-\Delta z)}$, $\bar{w}_e(z) = \frac{\sum_{i=1}^{N_e(z)} w_{ei}(z)}{N_e(z)}$, and $\bar{F}(z-\Delta z) = \sum_{i=1}^{N(z-\Delta z)} \int_{t(z-\Delta z)}^{t(z)} F(t)dt/N(z-\Delta z)$. Here $\bar{F}$ has the unit of velocity because it is integrated over time. Note that throughout the paper, the average operator denotes the average of all parcels within a parcel group rather than all parcel groups. We may therefore simplify equation (6) by writing

$$N(z)\bar{w}(z) = N(z-\Delta z)(\bar{w}(z-\Delta z) + \bar{F}(z-\Delta z)) + N_e(z)\bar{w}_e(z). \tag{7}$$

By rearranging terms, we can derive the following:

$$\bar{w}(z) - \bar{w}(z-\Delta z) = \frac{1}{N(z)}[N(z-\Delta z)\bar{F}(z-\Delta z) + N_e(z)(\bar{w}_e(z) - \bar{w}(z-\Delta z))]. \tag{8}$$

The first term on the r.h.s. represents accelerations, and the second term shows the effect of entrainment of environmental air with small vertical velocities on the updraft momentum budget. The convective response to a small perturbation, namely, the difference between the perturbed and control runs can be written in the following way:

$$\delta(\bar{w}(z) - \bar{w}(z-\Delta z)) = \delta(\frac{1}{N(z)}[N(z-\Delta z)\bar{F}(z-\Delta z) + N_e(z)(\bar{w}_e(z) - \bar{w}(z-\Delta z))]). \tag{9}$$

The change in the first term on the r.h.s. includes both the effect of entrainment on the thermodynamic properties (thus buoyancy) of cloudy updrafts and acceleration changes induced by the imposed temperature

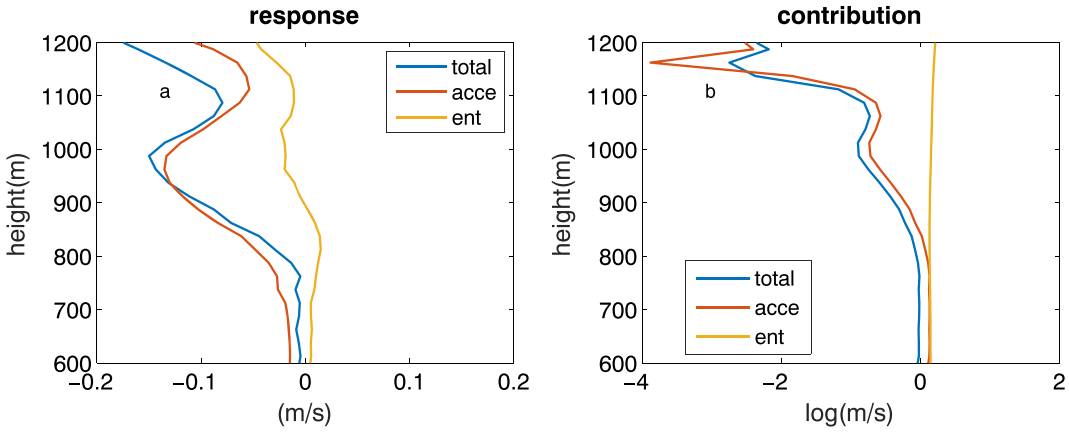


**Figure 4.** (a) Decomposition of convective response according to equation (9), blue(total) = $\delta(\bar{w}(z)-\bar{w}(z-\Delta z))$; red(acce) = $\delta(\frac{1}{N(z)}\sum_{N(z-\Delta z)}(N(z-\Delta z)\bar{F}(z-\Delta z))$; orange(ent) = $\delta(\frac{1}{N(z)}N_e(z)(\bar{w}_e(z)-\bar{w}(z-\Delta z)))$; (b) relative contribution from change in total acceleration (no dilution from entrainment included) based on equation (10): $\delta(\ln N(z-\Delta z)\bar{F}(z-\Delta z))$ and entrainment term: $-\delta(\ln N(z))$, the values here are taken logarithmic. For both figures, difference value is computed every 100 m in the vertical.

perturbation. The absolute magnitude of the second term on the r.h.s. of equation (8) is nonnegligible. However, its difference between control and perturbed run is much smaller compared to that of the first term (Figure 4a), indicating that entrainment mostly acts to dilute the accelerations to affect the vertical momentum budget. Divide both sides of equation (9) by their respective control run values and given the small second term, we can get

$$\begin{aligned}\delta(\ln(\bar{w}(z)-\bar{w}(z-\Delta z))) &= \delta(\ln(\frac{1}{N(z)}[N(z-\Delta z)\bar{F}(z-\Delta z)+N_e(z)(\bar{w}_e(z)-\bar{w}(z-\Delta z))]))\\ &\approx \delta(\ln N(z-\Delta z)\bar{F}(z-\Delta z))-\delta(\ln N(z)).\end{aligned} \tag{10}$$

It is then demonstrated (Figure 4b) that the change in cloudy updraft vertical velocity is mostly due to the buoyancy change: that a buoyancy barrier is formed to effectively reduce the kinetic energy of cloudy parcels, whereas the entrainment does not affect the momentum as much as the direct buoyancy effect. The results are consistent with de Roode et al. (2012) that entrainment is not the dominant sink in the vertical momentum budget.

If we multiply both sides of equation (8) by $\bar{w}(z-\Delta z)$ and divide it by $\Delta z$, we can obtain

$$\begin{aligned}\frac{\bar{w}(z-\Delta z)\Delta\bar{w}(z-\Delta z)}{\Delta z} = \frac{\bar{w}(z-\Delta z)}{N(z)\Delta z}[&N(z-\Delta z)\bar{F}(z-\Delta z)+\\ &N_e(z)(\bar{w}_e(z)-\bar{w}(z-\Delta z))],\end{aligned} \tag{11}$$

where we have defined $\Delta\bar{w}(z-\Delta z)=\bar{w}(z)-\bar{w}(z-\Delta z)$. Define $\tau=\frac{\Delta z}{\bar{w}(z-\Delta z)}$ to denote the average time that particles take to cross length $\Delta z$, and $\bar{F}_{all}(z-\Delta z)=\frac{1}{N(z)\tau}N(z-\Delta z)\bar{F}(z-\Delta z)$, which represents the total accelerations including both buoyancy and pressure gradient terms. Again, the average operator is over a particular parcel group. Equation (11) can now be simplified as

$$\begin{aligned}\frac{\bar{w}(z-\Delta z)\Delta\bar{w}(z-\Delta z)}{\Delta z} &= \bar{F}_{all}(z-\Delta z)+\frac{\bar{w}(z-\Delta z)N_e(z)}{N(z)\Delta z}(\bar{w}_e(z)-\bar{w}(z-\Delta z))\\ &\approx \bar{F}_{all}(z-\Delta z)-\epsilon(\bar{w}(z-\Delta z)^2),\end{aligned} \tag{12}$$

in which $\epsilon=\frac{N_e(z)}{N(z)\Delta z}$ is the fractional entrainment rate represented by the particles. We have neglected $\bar{w}_e(z)$ term in the second line since, as mentioned earlier, its magnitude is small. Taking the limit of small $\Delta z$, we have

$$\frac{1}{2}\frac{\partial\bar{w}^2}{\partial z}\approx\bar{F}_{all}-\epsilon\bar{w}^2. \tag{13}$$

We can further decompose the total acceleration term according to equation (3)

$$\bar{F}_{all} = \bar{B} - \frac{1}{\rho}\frac{d\bar{p}'_B}{dz} - \frac{1}{\rho}\frac{d\bar{p}'_M}{dz}. \tag{14}$$

Now rewriting equation (14) as

$$\frac{1}{2}\frac{\partial \bar{w}^2}{\partial z} = \bar{B} - \frac{1}{\rho}\frac{d\bar{p}'_B}{dz} - \frac{1}{\rho}\frac{d\bar{p}'_M}{dz} - \epsilon\bar{w}^2. \tag{15}$$

By adopting the term effective buoyancy $\bar{\beta} = \bar{B} - \frac{1}{\rho}\frac{d\bar{p}'_B}{dz} = a\bar{B}$, where a is the ratio between the effective buoyancy $\bar{\beta}$ and buoyancy $\bar{B}$ itself, that is, the so-called virtual mass coefficient, we have

$$\frac{1}{2}\frac{\partial \bar{w}^2}{\partial z} = a\bar{B} - \frac{1}{\rho}\frac{d\bar{p}'_M}{dz} - \epsilon\bar{w}^2. \tag{16}$$

In previous efforts to parameterize vertical velocity in convective schemes (e.g., Bretherton et al., 2004; Gregory, 2001; Simpson & Wiggert, 1969), the mechanically induced perturbation pressure and subgrid fluctuations are related to the entrainment term by defining b such that $-\frac{1}{\rho}\frac{d\bar{p}'_M}{dz} - \epsilon\bar{w}^2 = b\bar{w}^2$, and they altogether compose of the momentum sink of cloudy updrafts, whereas effective buoyancy serves as the source of vertical momentum. Therefore, equation (16) is a more general form of equation (1), derived from a Lagrangian perspective, without making the assumption that mechanically induced perturbation pressure gradient is related to the entrainment term. As mentioned earlier, the coefficients *a* and *b* are often determined using linear regressions and can vary substantially among different studies (de Roode et al., 2012). We shall explicitly calculate the value of virtual mass and mechanically induced perturbation pressure based on a rather simple cylindrical updraft model. While idealized calculations of the virtual mass is not new in this field (e.g., Davies-Jones, 2003; Jeevanjee & Romps, 2016; Morrison, 2016a, 2016b; Peters, 2016), we are not aware of attempts to apply this in the context of parameterizing the updraft vertical velocity (i.e., equation (1)).

The vertical profile of in-cloud buoyancy acceleration is given by LES, and we assume that buoyancy follows a Gaussian distribution in the horizontal directions, with the horizontal length scale being approximated by the cloud size (or cloud radius), which is an input to our simple model. And the cloud size is approximated by the average cloud radius in the LES simulation. Here the perturbation pressure terms are calculated with respect to the bulk plume, that is by summing up all individual parcel groups together to make a single plume, because pressure is a global rather than a local quantity. Based on this bulk updraft model, we calculate the buoyancy-induced perturbation pressure according to equation (4). We impose the Dirichlet boundary condition and integrate the equation from cloud base to cloud top in the vertical direction. After obtaining the buoyancy-induced perturbation pressure, we calculate the effective buoyancy and the coefficient *a*. Using this simple updraft geometry, we can almost reproduce the behavior of LES-diagnosed coefficient *a* by adjusting the cloud size parameter as shown in Figure 5.

Figure 5a shows the coefficient *a* computed by LES directly, and Figure 5b shows *a* values using our simplified updraft model with a fixed cloud size of 150 m (which is the typical cloud size in our shallow convection simulation). We can see that the main features of virtual mass coefficient *a* can be captured by our simple model to a good extent. The coefficient *a* is almost constant and ranges between 0.6 and 0.7 for the control run. The perturbed run value is larger than the control run at heights where the temperature perturbation is added. The peak *a* value occurs around the peak perturbation level in the perturbed run. While this peak is associated with an artificially localized perturbation, this result implies that *a* is not a constant value if there exists a strong local perturbation in the cloud layer, and we do not need to fix *a* to be a constant, as what is done in most existing vertical velocity parameterizations. Instead, we can calculate it from model-diagnosed buoyancy profile and cloud radius. The former variable is a standard output from most parameterizations, whereas cloud radius still needs to be investigated further, and is likely also needed for computing the entrainment rates (e.g., Tian & Kuang, 2016).

A similar approach based on an assumed cylindrical cloud geometry is taken to calculate the mechanically induced pressure gradient term as well. In order to calculate the $-\frac{1}{\rho}\frac{d\bar{p}'_M}{dz}$ term, we first derive the vertical

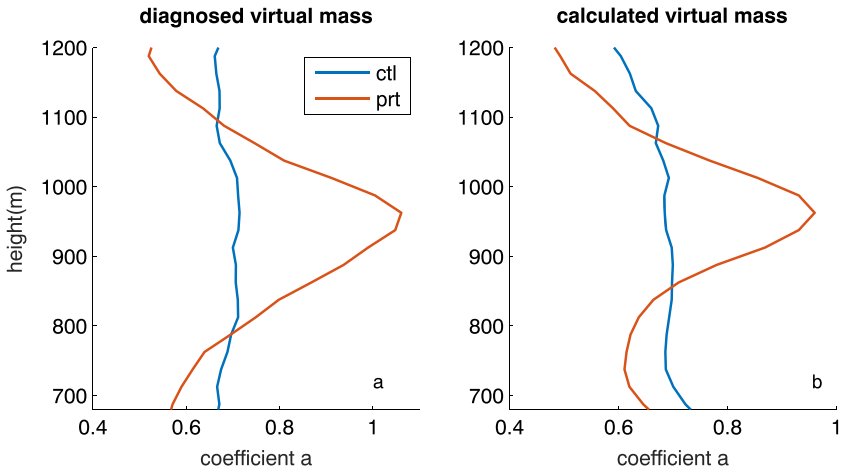


**Figure 5.** Coefficient $a$ as a function of height based on direct model output (a) and simple cartoon model (b) with a fixed radius of 150 m. What is shown here is the first term in the right-hand side of equation (16): $a\bar{B}$, and it is calculated for both control run (blue curve) and perturbed run (red curve) in each framework. This term represents the effective buoyancy that cloudy updrafts experience, in which Archimedean buoyancy ($\bar{B}$) is canceled by its induced pressure gradient term ($-\frac{1}{\rho}\frac{d\bar{p}'_M}{dz}$) to a certain extent.

velocity based on the vertical momentum equation without $-\frac{1}{\rho}\frac{d\bar{p}'_M}{dz}$. The horizontal velocities $u$ and $v$ are calculated assuming nondivergent axisymmetric flow and a known cloud size. Again, the horizontal distribution of vertical velocity at each level is assumed to be Gaussian. Then the pressure gradient term can be obtained from equation (5) once horizontal velocities are known, and the results are shown in Figure 6. This simple model only needs the buoyancy profile and cloud radius as inputs, and thus could be used as a parameterization.

Figure 6b illustrates the mechanically induced pressure gradient term calculated from the updraft model and the corresponding LES-diagnosed results (Figure 6a). The general feature and relative magnitude of mechanical accelerations are well reproduced. However, this simple model cannot represent the exact changes in the perturbed run relative to the control run, and the calculated mechanical acceleration seems to be a bit larger than the LES-diagnosed one. To evaluate the utility of the simple updraft model under more general conditions, we also performed the same analyses for deep convection in a radiative convective equilibrium state. We computed both the virtual mass coefficients and mechanically induced perturbation

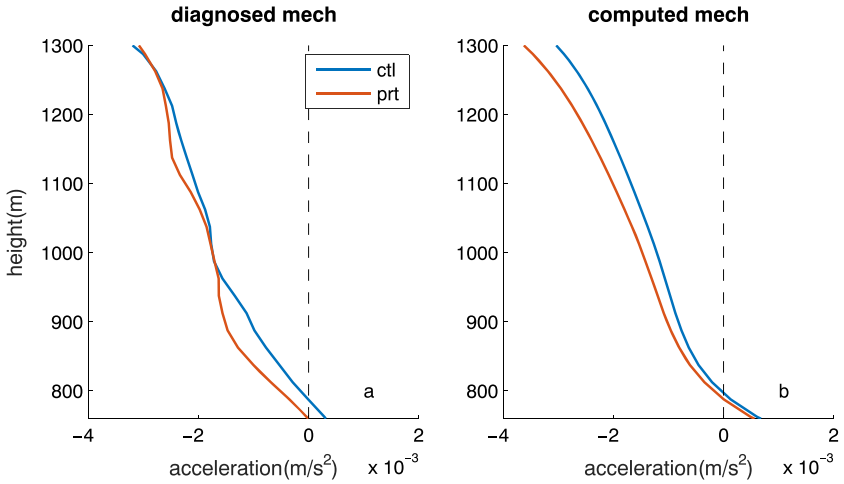


**Figure 6.** Mechanical acceleration based on direct model output (a) and simple cartoon model (b). What is shown here is the second term in the right-hand side of equation (16): $-\frac{1}{\rho}\frac{d\bar{p}'_M}{dz}$, and it is calculated for both control run (blue curve) and perturbed run (red curve) in each framework.

pressures for the radiative convective equilibrium case. The simple cylindrical updraft model can capture the basic features well given reasonable cloud radii (see supporting information for results).

For both shallow and deep convection, our simple cloud model captures the virtual mass coefficients better than the mechanical acceleration term. There may be several possible reasons for this: the ensemble number is small, therefore the result can be noisy; the assumed axisymmetric cylinder shape does not work well for mechanical acceleration compared to buoyancy since the former can be more spatially heterogeneous than the later, which implies that a more complicated treatment might be needed to fully account for the dynamic perturbation pressure as in Morrison (2016a) and Peters (2016); our simple model neglects the influence from the subcloud layer, and this might be of greater importance for the mechanical acceleration than the buoyancy force. We will further address subcloud layer and convective organization in the future work. Nevertheless, this deterministic cartoon approach is still promising. In particular, it may be useful in developing a unified convective parameterization scheme for both shallow and deep convection without having to arbitrarily choose coefficients for parameterizing vertical momentum in each individual case.

## 4. Summary and Discussions

A new approach is proposed to diagnose the relative importance of various forcing terms in the vertical momentum budget. This approach reveals that the total mechanical forcing plays an equally important role as the total buoyancy forcing in the momentum budget of cloudy updrafts, whereas, consistent with de Roode et al. (2012), Sherwood et al. (2013), Romps and Charn (2015), and so forth, the effect of entrainment dilution is relatively weak. This is consistent with both Sherwood et al. (2013) and Romps and Charn (2015), although these studies came to opposing conclusions as to the importance of drag for cloud thermals. In particular, Sherwood et al. (2013) focused on the "drag" due to entrainment dilution, which we have shown to be relatively weak, while Romps and Charn (2015) included form and wave drag, finding that these terms were comparable to the size of the buoyancy. Therefore, if we define drag to include form drag, as represented by the perturbation pressure gradient force, our study confirms that updrafts should be considered to be sticky. Our analysis further distinguishes between the two components of the nonhydrostatic pressure gradients, namely, the buoyancy-induced part and the mechanically induced part explicitly, and quantifies the relative importance of each component. It is shown that the mechanically induced drag term is equally important as the buoyancy-induced part. Both Sherwood et al. (2013) and Romps and Charn (2015) track individual thermals delineated by some boundaries, our study looks directly at cloudy updrafts from a cumulus ensemble perspective, which can be more applicable to velocity parameterization in convective schemes. Based on the dominant force balance in the vertical momentum budget, we further explore the potential of employing a rather simple cloud model to explicitly calculate various factors without predefining empirical coefficients $a$ and $b$ as what has been done in most existing convective parameterization schemes that include an updraft vertical velocity equation. We have explicitly calculated the virtual mass coefficient and dynamical perturbation pressure based on a simple cylindrical geometry and cloud radius assumption, which could be useful in parameterizing vertical velocity in convective schemes. Combined with the entrainment formula proposed in Tian and Kuang (2016) in which vertical velocity and cloud radius are needed to determine the entrainment rate, this has the potential to make a self-contained convective parameterization. However, this approach is heavily dependent upon the knowledge of cloud size, the determination of which is beyond the scope of this current study, and further investigations will be conducted on this aspect. Furthermore, the subcloud influence is not considered in the current study, which could impact the estimates of perturbation pressure terms, which will also be discussed in detail in the future work.

**Acknowledgments**
This research was partially supported by the Office of Biological and Environmental Research of the U.S. DOE under grant DE-SC0018120 as part of the ASR Program and NSF grant AGS-1649819. The Harvard Odyssey cluster provided much of the computing resources for this study. The authors also thank Marat Khairoutdinov for making the SAM model available. The numerical model was developed by M. Khairoutdinov and can be obtained at http://rossby.msrc.sunysb.edu/marat/SAM.html. All input files for the numerical simulations are available upon requests.

## References

Arakawa, A., & Schubert, W. H. (1974). Interaction of a cumulus cloud ensemble with the large-scale environment. Part I. *Journal of the Atmospheric Sciences*, *31*, 674–701.

Bretherton, C. S., McCAA, J. R., & Grenier, H. (2004). A new parameterization for shallow cumulus convection and its application to marine subtropical cloud-topped boundary layers. Part I: Description and 1D results. *Monthly Weather Review*, *132*, 864–882.

Danielsen, E. F., Bleck, R., & Morris, D. A. (1972). Hail growth by stochastic collection in a cumulus model. *Journal of the Atmospheric Sciences*, *29*, 135–155.

Davies-Jones, R. (2003). An expression for effective buoyancy in surroundings with horizontal density gradients. *Journal of the Atmospheric Sciences*, *60*, 2922–2925.

Dawe, J. T., & Austin, P. H. (2013). Direct entrainment and detrainment rate distributions of individual shallow cumulus clouds in an LES. *Atmospheric Chemistry and Physics*, *13*, 7795–7811.

de Roode, S. R., Siebesma, A. P., Jonker, J. J., & Voogd, Y. D. (2012). Parameterization of the vertical velocity equation for shallow cumulus clouds. *Monthly Weather Review*, *140*, 2424–2436.

De Rooy, W. C., & Siebesma, A. P. (2010). Analytical expressions for entrainment and detrainment in cumulus convection. *Quarterly Journal of the Royal Meteorological Society*, *136*, 1216–1227.

Gregory, D. (2001). Estimation of entrainment rate in simple models of convective clouds. *Quarterly Journal of the Royal Meteorological Society*, *127*, 53–72.

Heus, T. (2008). Mixing in shallow cumulus clouds studied by Lagrangian particle tracking. *Journal of the Atmospheric Sciences*, *65*, 2581–2597.

Holland, J. Z., & Rasmusson, E. M. (1973). Measurement of atmospheric mass, energy, and momentum budgets over a 500-kilometer square of tropical ocean. *Monthly Weather Review*, *101*, 44–55.

Houze, R. (1994). *Cloud dynamics, Int. Geophys.* New York: 53 Academy Press.

Hsu, J, & Prather, M. (2014). Is the residual vertical velocity a good proxy for stratosphere-troposphere exchange of ozone? *Geophysical Research Letters*, *41*, 9024–9032. https://doi.org/10.1002/2014GL061994

Jeevanjee, N, & Romps, D. (2016). Effective buoyancy at the surface and aloft. *Quarterly Journal of the Royal Meteorological Society*, *142*, 811–820.

Khairoutdinov, M. F., & Randall, D. A. (2001). A cloud-resolving model as a cloud parameterization in the NCAR Community Climate System Model: Preliminary results. *Geophysical Research Letters*, *28*, 3617–3620.

Kuang, Z. (2010). Linear response functions of a cumulus ensemble to temperature and moisture perturbations and implication to the dynamics of convectively coupled waves. *Journal of the Atmospheric Sciences*, *67*, 941–962.

Kuang, Z., & Bretherton, S. C. (2006). A mass-flux scheme view of a high-resolution simulation of a transition from shallow to deep cumulus convection. *Journal of the Atmospheric Sciences*, *63*, 1895–1909.

Lin, C., & Arakawa, A. (1997). The macroscopic entrainment processes of simulated cumulus ensemble. Part II: Testing the entraining-plume model. *Journal of the Atmospheric Sciences*, *54*, 1044–1053.

Morrison, H. (2016a). Impacts of updraft size and dimensionality on the perturbation pressure and vertical velocity in cumulus convection. Part I: Simple, generalized analytic solutions. *Journal of the Atmospheric Sciences*, *73*, 1441–1454.

Morrison, H. (2016b). Impacts of updraft size and dimensionality on the perturbation pressure and vertical velocity in cumulus convection. Part II: Comparison of theoretical and numerical solutions and fully dynamical simulations. *Journal of the Atmospheric Sciences*, *73*, 1455–1480.

Morton, B., Taylor, G., & Turner, J. (1956). Turbulent gravitational convection from maintained and instantaneous sources. *Proceedings of the Royal Society of London*, *234*, 1–23.

Neggers, R., Kohler, A. M., & Beljaars, A. (2009). A dual mass flux framework for boundary layer convection. Part I: Transport. *Journal of the Atmospheric Sciences*, *59*, 1655–1668.

Nie, J., & Kuang, Z. (2012a). Responses of shallow cumulus convection to large-scale temperature and moisture perturbations: A comparison of large-eddy simulations and a convective parameterization based on stochastically entraining parcels. *Journal of the Atmospheric Sciences*, *69*, 1936–1956.

Nie, J., & Kuang, Z. (2012b). Beyond bulk entrainment and detrainment rates: A new framework for diagnosing mixing in cumulus convection. *Geophysical Research Letters*, *39*, L21803. https://doi.org/10.1029/2012GL053992

Peters, J. (2016). The impact of effective buoyancy and dynamic pressure forcing on vertical velocities within two-dimensional updrafts. *Journal of the Atmospheric Sciences*, *73*, 4531–4551.

Price, C., & Rind, D. (1992). A simple lightning parameterization for calculating global lightning distributions. *Journal of Geophysical Research*, *97*, 9919–9933.

Romps, D. M. (2010). A direct measure of entrainment. *Journal of the Atmospheric Sciences*, *67*, 1908–1927.

Romps, D. M., & Charn, A. (2015). Sticky thermals: Evidence for a dominant balance between buoyancy and drag in cloudy updrafts. *Journal of the Atmospheric Sciences*, *72*, 2890–2901.

Romps, D. M., & Kuang, Z. (2010). Do undiluted convective plumes exist in the upper tropical troposphere. *Journal of the Atmospheric Sciences*, *67*, 468–484.

Sherwood, S. C., Hernandez-Deckers, D., Colin, M., & Robinson, F. (2013). Slippery thermals and the cumulus entrainment paradox. *Journal of the Atmospheric Sciences*, *70*, 2426–2442.

Siebesma, A. P., Soares, P. M. M., & Teixeira, J. (2007). A combined eddy-diffusivity mass-flux approach for the convective boundary layer. *Journal of the Atmospheric Sciences*, *64*, 1230–1248.

Simpson, J., & Wiggert, V. (1969). Models of precipitating cumulus towers. *Monthly Weather Review*, *97*, 471–489.

Soares, P. M. M., Miranda, P. M. A., Siebesma, A. P., & Teixeira, J. (2004). An eddy-diffusivity/massflux parametrization for dry and shallow cumulus convection. *Quarterly Journal of the Royal Meteorological Society*, *130*, 3365–3383.

Tian, Y., & Kuang, Z. (2016). Dependence of entrainment in shallow cumulus convection on vertical velocity and distance to cloud edge. *Geophysical Research Letters*, *43*, 4056–4065. https://doi.org/10.1002/2016GL069005

Tian, Y., & Kuang, Z. (2018). Why does deep convection have different sensitivities to temperature perturbations in the lower and upper troposphere. *Journal of the Atmospheric Sciences*, *76*, 27–41.

Tiedtke, M. (1989). A comprehensive mass flux scheme for cumulus parameterization in large-scale models. *Monthly Weather Review*, *117*, 1779–1800.

Tompkins, A., & Craig, G. C. (1998). Time-scales of adjustment to radiative-convective equilibrium in the tropical atmosphere. *Quarterly Journal of the Royal Meteorological Society*, *124*, 2693–2713.

Torri, G., Kuang, Z., & Tian, Y. (2015). Mechanisms for convection triggering by cold pools. *Geophysical Research Letters*, *42*, 1943–1950. https://doi.org/10.1002/2015GL063227

Tulich, S., & Mapes, B. E. (2010). Transient environmental sensitivities of explicitly simulated tropical convection. *Journal of the Atmospheric Sciences*, *697*, 923–940.

Weil, J. C. (2004). The use of large-eddy simulation in Lagrangian particle dispersion models. *Journal of the Atmospheric Sciences*, *61*, 2877–2887.

Williams, E. R., Weber, M. E., & Orville, R. E. (1989). The relationship between lightning type and convective state of thunderclouds. *Journal of Geophysical Research*, *94*, 13,213–13,220.

Yeo, K., & Romps, D. (2013). Measurement of convective entrainment using Lagrangian particles. *Journal of the Atmospheric Sciences*, *70*, 266–277.